Available online at www.sciencedirect.com
ScienceDirect
Trans. Nonferrous Met. Soc. China 22(2012) 2334−2342
Transactions of Nonferrous Metals Society of China
www.tnmsc.cn

Effect of microstructure on impact toughness of magnesium alloys

HUANG Zheng-hua, QI Wen-jun, XU Jing

Guangzhou Research Institute of Nonferrous Metals, Guangzhou 510650, China

Received 9 July 2012; accepted 2 August 2012

Abstract: Microstructures of as-cast and extruded ZK60−*x*RE (RE=Dy, Ho and Gd, *x*=0−5, mass fraction) alloys were investigated. Meanwhile, the impact toughness was tested and then the relationship was discussed. The results show that as-cast microstructure is refined gradually with increasing the RE content. Mg−Zn−RE new phase increases gradually, while $MgZn_2$ phase decreases gradually to disappear. Second phase tends to distribute along grain boundary in continuous network. Extruded microstructure is refined obviously to reach the micron level. Broken second phase tends to distribute along the extrusion direction in zonal shape. Impact toughness value α_{nK} increases from 9−17 J/cm^2 for as-cast state to 26−54 J/cm^2 for extruded state. With increasing the value of α_{nK}, fracture macro-morphology changes from a rough plane via multi-plane with step to V-type plane; and from single radiation zone to two zones of fiber and shear lip, respectively. Fracture micro-morphology changes from the brittle fracture to the ductile fracture. Fine grain and few fine dispersed second phase can enhance the impact toughness of magnesium alloys effectively.
Key words: ZK60 magnesium alloys; rare earth; alloying; impact toughness; microstructure; fracture morphology

1 Introduction

Magnesium alloy, one of the most important structural materials having high specific strength, is widely used in automotive, communication, electronic and aerial industries [1]. An alloy as a structural component should possess not only sufficient static strength but also superior dynamic property, since the failure of component is usually due to the dynamic loading against the foreign object during the service.

Impact toughness, an important dynamic mechanical property for engineering structural materials, can affect the performance and structural reliability significantly. Compared with steel [2,3] and aluminum alloys [4−6], the investigation on the impact toughness of magnesium alloys is lacking [7−13]. Impact toughness of AZ80 alloy decreases gradually with increasing the aging temperature and the fracture is quasi-cleavage [7]. Ductile-brittle transition phenomena exist in the temperature range from 393 K to 433 K for AZ31 alloy [8]. Magnesium alloys generally exhibit relatively poor impact toughness, thus it is necessary to enhance the impact toughness by studying the internal affecting factors such as the texture structure, grain size, second phase and impurity defects. LIAO et al [9] found that the impact toughness of extruded AZ31B alloy was enhanced significantly when the average grain size $\bar{d}$ is less than 3 μm and thought that fine grain was the main reason for improving the dynamic strength and plastic deformation ability. However, the role of other factors especially the second phase has not been investigated systematically yet. Therefore, the present work is focused on studying the microstructure of as-cast and extruded ZK60−*x*RE (RE=Dy, Ho and Gd) alloys with low and high RE contents, respectively, mainly discussing the common effects of grain size and second phase on the impact toughness value and fracture morphology, and then proposing an approach to obtain new magnesium alloys with high impact toughness in view of the two aspects.

2 Experimental

ZK60−*x*RE alloy ingots were prepared by melting pure Mg, pure Zn and Mg−30%Zr, Mg−30%RE master alloys in electric resistance furnace under the mixed atmosphere of CO_2 and SF_6. When the melt temperature of pure Mg reached 1003 K, pure Zn and master alloys were added into the melt in turn. Then, the melt was stirred twice within 1 h to ensure the compositional homogeneity. After adding the refining agent (JDMJ), the melt was held at 1033 K for 30 min. When the temperature was cooled to 988 K, the melt was poured into the wedge permanent mold with preheated temperature of 523 K, and then as-cast samples were

Foundation item: Projects (2010A090200078, 2011A080403008) supported by the Major Science and Technology Project of Guangdong Province, China
Corresponding author: HUANG Zheng-hua; Tel/Fax: +86-20-37238039; E-mail: zhhuang@live.cn
DOI: 10.1016/S1003-6326(11)61468-4

obtained. Cast rods obtained under the same technology were homogenized at 673 K for 8 h in the heat-treating furnace. Extrusion rods were obtained by extruder with extrusion ratio λ of 40, extrusion temperature of 593 K and extrusion speed v of 1−2 m/min, respectively.

The as-cast and extruded specimens were etched with 4% HNO_3 (volume fraction) in ethanol and a solution of 1.5 g picric acid, 25 mL ethyl alcohol, 5 mL acetic acid plus 10 mL distilled water, respectively. Microstructural observation was carried out on optical microscope (OM, Leica DM IRM), scanning electron microscope (SEM, JEOL JXA-8100) and transmission electron microscope (TEM, Tecnai G^2 20), respectively. Phase analysis was carried out on X-ray diffractometer (XRD, D/MAX-RC) with Cu K_α radiation. Phase change during the heating process was characterized by isochronally heating in differential scanning calorimeter (DSC, Netzsch STA409) under flow of highly-purified Ar atmosphere at a heating rate of 20 K/min. Standard un-notched impact specimen with dimension of 10 mm×10 mm×55 mm was tested on the pendulum impact testing machine at ambient temperature. Fractograph was observed using SEM.

3 Results and discussion

3.1 Microstructure

Figure 1 shows the optical and SEM graphs of

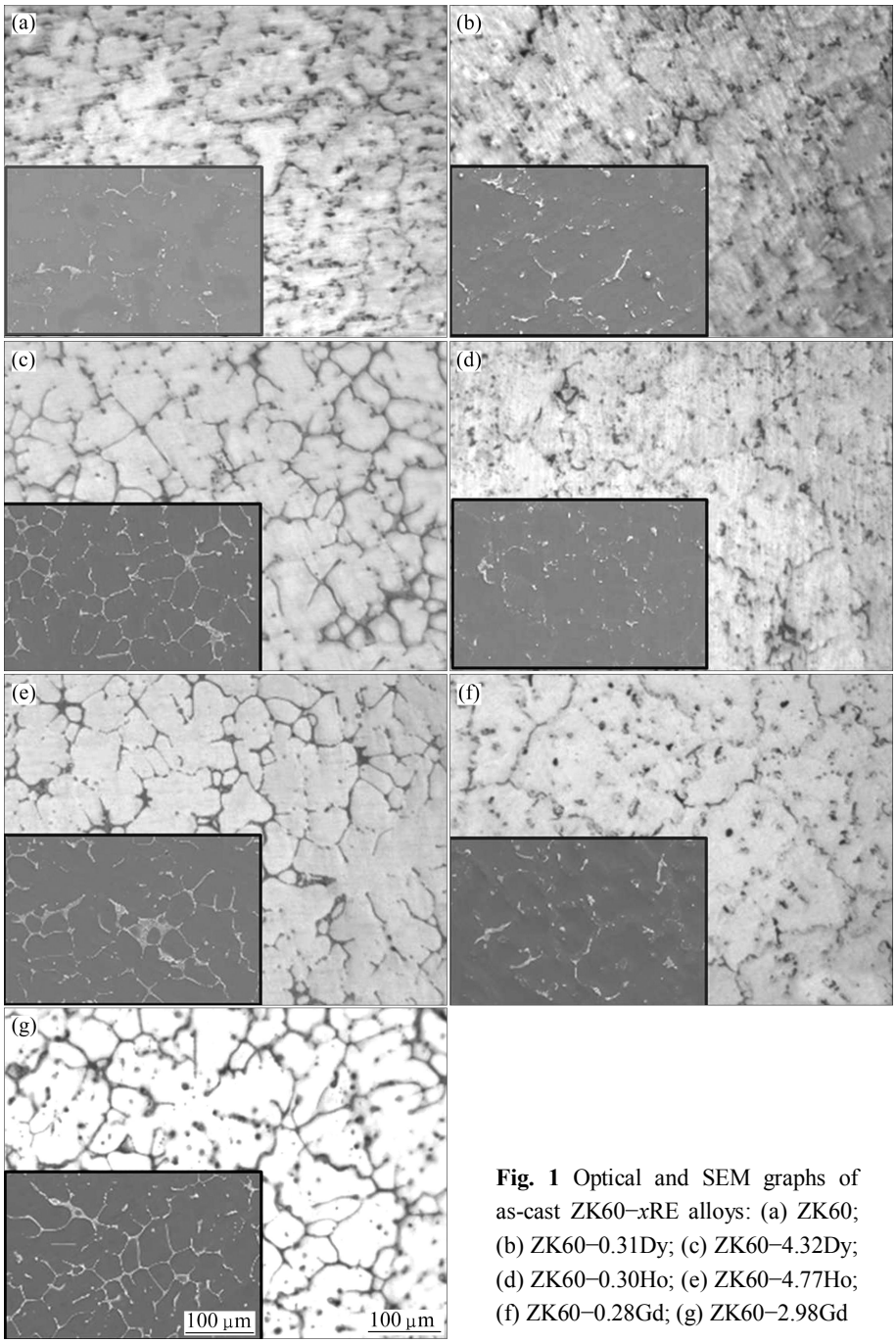

Fig. 1 Optical and SEM graphs of as-cast ZK60−xRE alloys: (a) ZK60; (b) ZK60−0.31Dy; (c) ZK60−4.32Dy; (d) ZK60−0.30Ho; (e) ZK60−4.77Ho; (f) ZK60−0.28Gd; (g) ZK60−2.98Gd

as-cast alloys. As-cast ZK60 alloy exhibits coarse microstructure and few dispersed second phase. With increasing the RE content, as-cast microstructure is refined gradually, meanwhile second phase increases gradually and tends to distribute along grain boundary in continuous network. The change of the grain size and second phase is almost similar for the three RE elements. Grain refinement mechanism for magnesium alloys is different with different grain-refining methods; however, the basic starting point is to increase the nucleation rate and inhibit the growth of crystal nuclei. Role of solute element can be expressed by growth restriction factor $m(k-1)$ [14]. The greater the value is, the stronger the refinement ability is. RE element exhibits relatively large value of $m(k-1)$, i.e. 4.64−5.52, thus the as-cast microstructure is refined effectively.

In order to determine new phase formation owing to the addition of RE, the comparison of the XRD patterns between as-cast ZK60 and ZK60−xRE alloys with high RE content was made (see Fig. 2(a)). XRD pattern of as-cast ZK60 alloy consists of the peaks of α-Mg and $MgZn_2$ phases, while the peak of $MgZn_2$ phase disappears completely and that of an unknown phase, not Mg−RE binary phase, can be observed among the XRD patterns of as-cast ZK60−xRE alloys with high RE content. Combined with the EDS results (not shown here), the unknown phase is considered as Mg−Zn−RE phase. Degree of difficulty in forming compounds between different elements can be judged by electronegativity difference $\Delta\chi$. The greater the value of $\Delta\chi$ is, the larger the binding force is, and then the easier the formation of compounds is [15]. Electronegativity χ is 1.31, 1.65 and 1.20−1.23 for Mg, Zn and RE elements, respectively [16], thus Zn−RE exhibits the larger value of $\Delta\chi$ (0.42−0.45) than Mg−Zn and Mg−RE (0.34 and 0.08−0.11, respectively), which leads to greater binding force between Zn and RE. Therefore, the RE atoms added combine with Zn and Mg atoms to form Mg−Zn−RE new phase on the priority.

Figure 2(b) shows the isochronal heating DSC curves of as-cast alloys. For as-cast ZK60 alloy, there exist two distinct endothermic peaks with peak temperatures T_{P1} and T_{P2} of 618 and 902 K, which are close to the melting point T_m (620 and 923 K) of $MgZn_2$ phase and α-Mg matrix, respectively. Thus, the two endothermic peaks should be corresponding to the melting of the two phases, respectively. For as-cast ZK60−xRE alloys with high RE content, the endothermic peak at T_P=618 K disappears completely and two or three new ones occur in the peak temperature range from 718 K to 871 K. These new endothermic peaks should be corresponding to the melting of Mg−Zn−RE phase. This

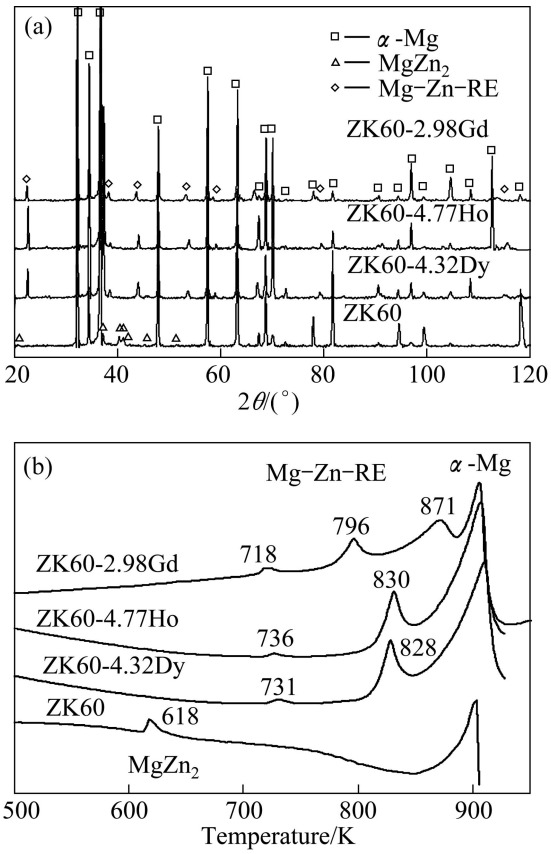

Fig. 2 XRD patterns (a) and isochronal heating DSC curves (b) of as-cast ZK60−xRE alloys

indicates that Mg−Zn−RE phase exhibits higher thermal stability than $MgZn_2$ phase.

Figures 3 and 4 show the optical, SEM and TEM images of extruded alloys, respectively. Compared with the as-cast microstructure, the extruded microstructure is refined significantly owing to the dynamic recrystallization under the condition of large deformation degree and middle deformation temperature. For the extruded ZK60 alloy, dynamic recrystallization grains (DRGs) change at a size range from 2 μm to 10 μm with the average grain size of 5 μm. Meanwhile, the majority of $MgZn_2$ phase dissolved through homogenization does not re-precipitate during the hot deformation process. With increasing the RE content, DRGs become unique and the average grain size gradually decreases to 1−2 μm for the extruded ZK60−xRE alloys with high RE content. The broken second phase distributes dispersedly for the extruded ZK60−4.32Dy and ZK60−4.77Ho alloys; however, it distributes along the extrusion direction in zonal shape for the extruded ZK60−2.98Gd alloy.

3.2 Impact toughness and fracture morphology

Figure 5 shows the impact toughness value α_{nK} of as-cast and extruded alloys. It is seen that α_{nK} on the

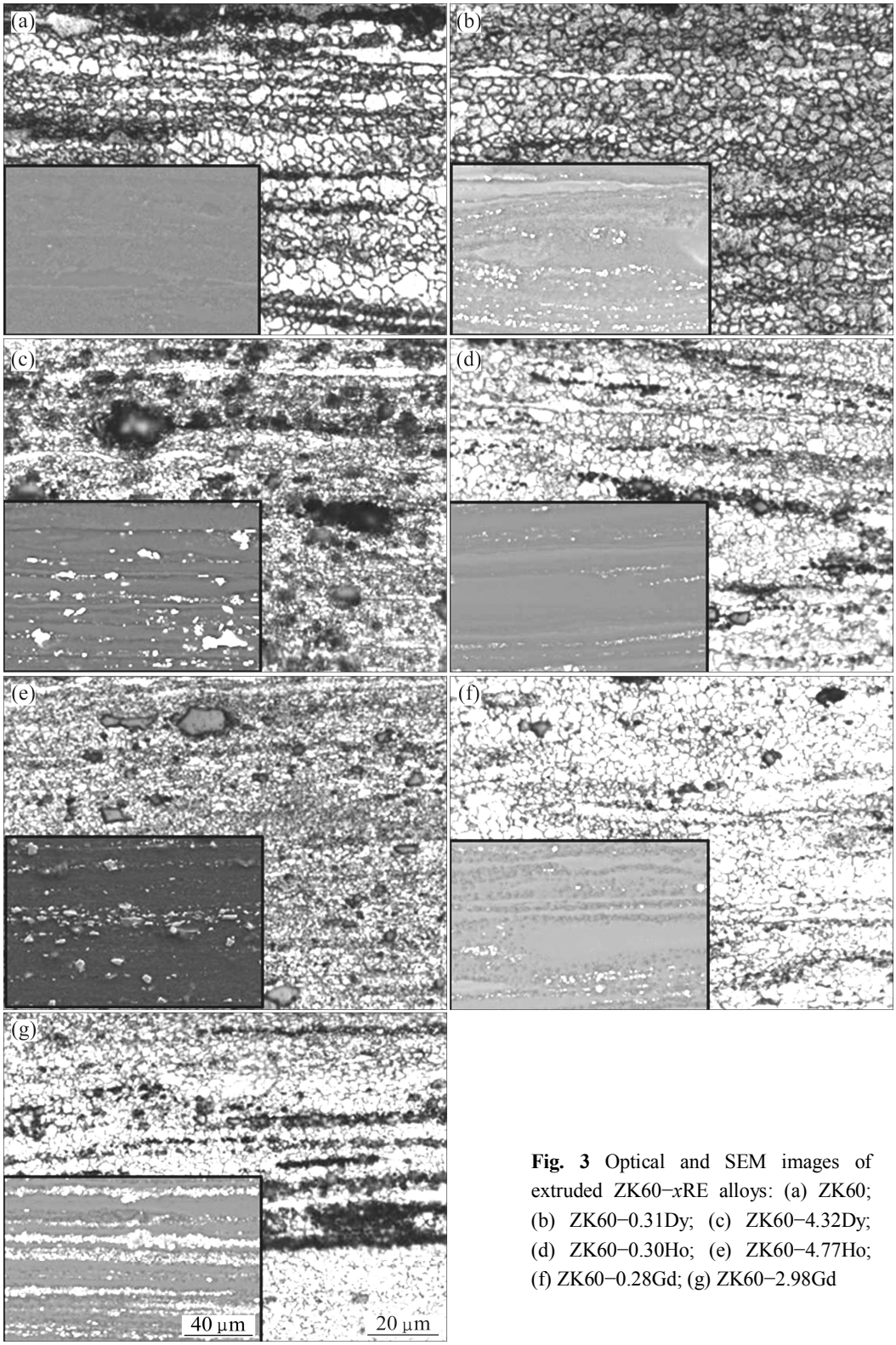

Fig. 3 Optical and SEM images of extruded ZK60−*x*RE alloys: (a) ZK60; (b) ZK60−0.31Dy; (c) ZK60−4.32Dy; (d) ZK60−0.30Ho; (e) ZK60−4.77Ho; (f) ZK60−0.28Gd; (g) ZK60−2.98Gd

whole is low for as-cast alloys. It first increases slightly from 13 J/cm^2 for as-cast ZK60 alloy to 15−17 J/cm^2 for as-cast alloys with low RE content, and then decreases to 9−10 J/cm^2 for as-cast alloys with high RE content, being even lower than that of the base alloy. After extrusion, the impact toughness is enhanced effectively. However, with increasing the RE content, α_{nK} decreases gradually from 54 J/cm^2 for extruded ZK60 alloy to 36, 26 and 28 J/cm^2 for the extruded ZK60−4.32Dy, ZK60−4.77Ho and ZK60−2.98Gd alloys, respectively.

Meanwhile, the fracture macro-morphology is related to the value of α_{nK} (Fig. 6). When α_{nK} <26 J/cm^2

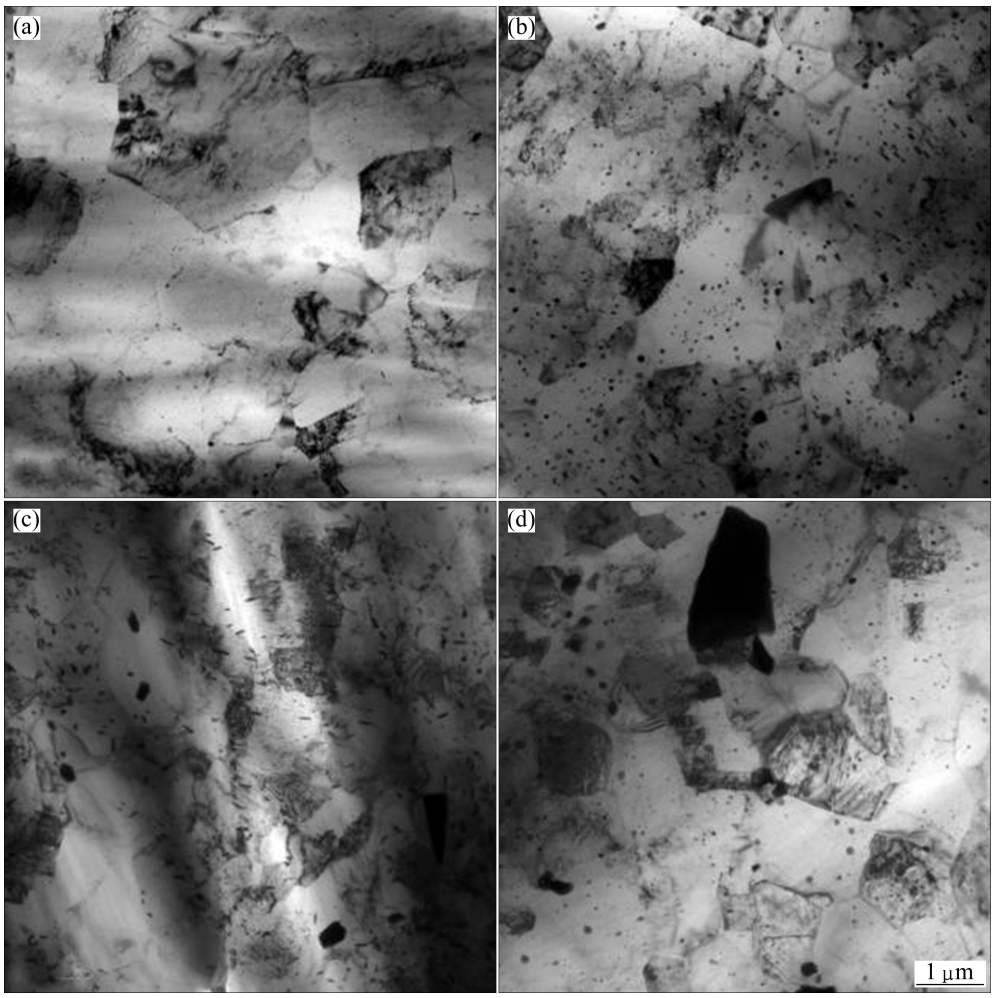

Fig. 4 TEM images of extruded ZK60−*x*RE alloys: (a) ZK60; (b) ZK60−4.32Dy; (c) ZK60−4.77Ho; (d) ZK60−2.98Gd

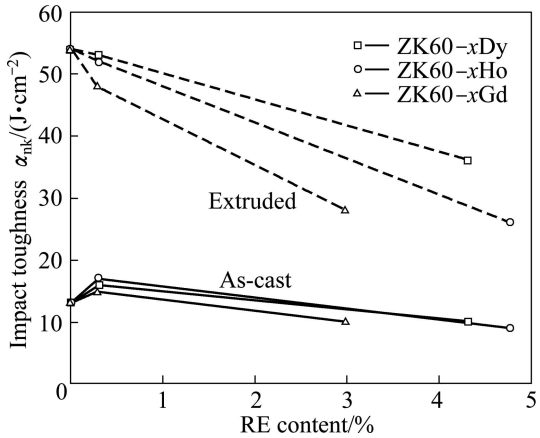

Fig. 5 Impact toughness value α_{nK} of as-cast and extruded ZK60−*x*RE alloys

for all as-cast alloys, the impact fracture exhibits a rough plane, where radiation zone is predominant and other two zones of fiber and shear lip can hardly be observed with naked eyes (Fig. 6(a)). When 26 J/cm^2≤α_{nK}<36 J/cm^2, the impact fracture tends to become multi-plane with step in the middle region. Shear lip zone can be observed

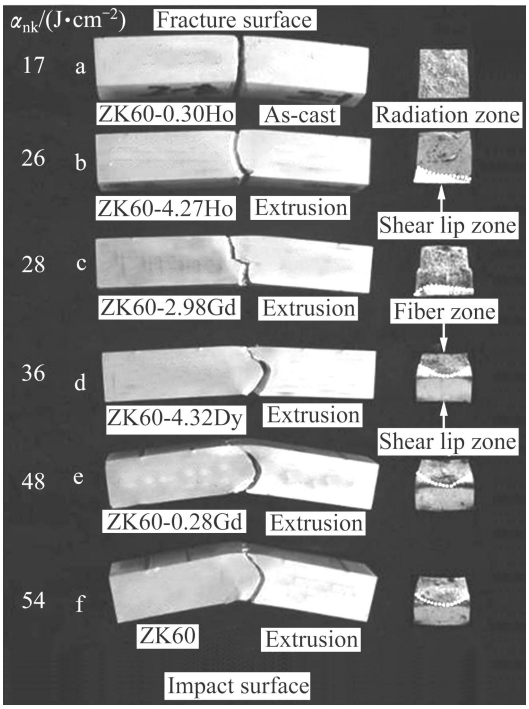

Fig. 6 Fracture macrographs of as-cast and extruded ZK60−*x*RE alloys

clearly near the impact surface where the cutting edge of pendulum first contacts the specimen. The region adjacent to the fracture surface where crack initiates transforms into fiber zone gradually (Figs. 6(b) and (c)). When $\alpha_{nK}\geq 36$ J/cm^2 for the majority of extruded alloys, the impact fracture changes to V-type plane with angle of approximately 120°, and meanwhile, the flexion degree of specimen increases gradually. Shear lip zone expands to the whole bottom half-region as well as a small scale between two sides on adjacent upper half-region, which is fiber zone (see dashed lines in Figs. 6(d)−(f)).

Crack generally initiates at the bottom of the notch or sub-surface adjacent to the fracture surface for the un-notched specimen. For alloys and materials, crack first propagates stably along two sides and depth direction to form fiber zone with protrusion, then propagates unstably to form radiation zone, and finally shear lip zone is formed. Plastic deformation ability can generally be estimated by the relative proportion of the three regions. The larger the fiber zone is, the better the plasticity is [17]. It is possible to observe only two zones of fiber and shear lip (Figs. 6(d)−(f)). As plasticity reduces, radiation zone expands gradually (Fig. 6(a)).

Figure 7 shows the fracture SEM morphologies of the as-cast and extruded alloys. For as-cast alloys, the rough impact fracture exhibits the complex mode of brittle and ductile fractures. Crack source can be observed clearly near the fracture surface (see arrow in Fig. 7(a)). As the region is approaching to the impact surface, equiaxed dimples resulting from tensile stress increase slightly. Shear lip zone can only reach 10−30 μm in width (Figs. 7(a)−(c)). For the extruded ZK60−4.77Ho alloy, the relatively smooth impact fracture changes to a typical feature of ductile fracture. No clear crack source can be observed. Relatively deep equiaxed dimples are predominant and many second phase particles can be observed clearly at the bottom of the equiaxed dimples (Fig. 7(d)). Equiaxed dimples become shallow and some cracks can be observed in the middle region (arrows in Fig. 7(e)). Wider shear lip zone exhibits elongated dimples caused by tear stress and meanwhile adjacent equiaxed dimples become deeper (Fig. 7(f)). For the extruded ZK60−2.98Gd alloy with multi-plane, the fracture surface exhibits more elongated dimples and less second phase particles at the bottom of equiaxed dimples (Fig. 7(g)). However, the micro-morphologies of the bench region and shear lip zone on the whole are similar to those of the former alloy (Figs. 7(h) and (i)). For the extruded ZK60−4.32Dy alloy with V-type plane, elongated dimples increase significantly near the smoother fracture surface and second phase particles reduce further (Fig. 7(j)). A certain amount of equiaxed dimples still exist in the upper region adjacent to the junction, while the bottom one has changed to the completely elongated dimples (Fig. 7(k)). As the region is approaching to the impact surface, the elongated dimples become smoother (Fig. 7(l)). With increasing the value of α_{nK} further, the whole impact fracture becomes smoother (Figs. 7(m)−(o)).

The formation of V-type impact fracture (Figs. 6(d)−(f)) can be described as follows simply. When the cutting edge of pendulum first contacts the specimen, the region without crack is large enough to form the tensile stress at the local region near the fracture surface, and then equiaxed dimples are formed. As crack propagates, the un-cracked region becomes smaller, which can make the tensile stress weakened and the tear stress strengthened, respectively. Meanwhile, crack propagates by an angle along the specimen axis under the interaction of the two stresses. When crack propagates to the middle region of specimen, tear stress begins to be predominant and accordingly the elongated dimples are predominant. Meanwhile, crack begins to propagate by another opposite direction. As crack propagates further, the elongated dimples increase gradually and become smoother owing to the strengthened tear stress.

3.3 Dependence of impact toughness on microstructure

Compared with the elastic deformation during the impact process, plastic deformation reflected by the crack initiation and propagation is predominant for magnesium alloys. Among the internal affecting factors, grain refinement can make the impurity concentration on grain boundary decrease, and then the brittle fracture weakens. Impediment of grain boundary is large when plastic deformation crosses from one grain to another grain. Meanwhile, the change in the sliding direction can consume more energy when crack passes through the grain boundary. Therefore, alloys with fine grain should exhibit high impact toughness. Compared with the matrix, the second phase generally precipitating along grain boundary may become the place of crack initiation more easily owing to the un-synchronous plastic deformation. The harmful effect can be weakened effectively by few fine dispersed second phase. In addition, impurity defects along grain boundary increase the tendency to intergranular fracture, and ones within the grain also become the place for crack initiation.

Although as-cast microstructure is refined gradually with increasing the RE content, all grain size exceeds 40 μm (Fig. 1), which leads to low impediment during the impact process. Meanwhile, second phase tending to distribute along grain boundary in continuous network can make crack initiate along the interface easily. Thus, all as-cast alloys exhibit the low value of α_{nK}. After adding low RE content, the dissolution of few RE atom in the matrix can enhance its strength slightly. Thus, α_{nK}

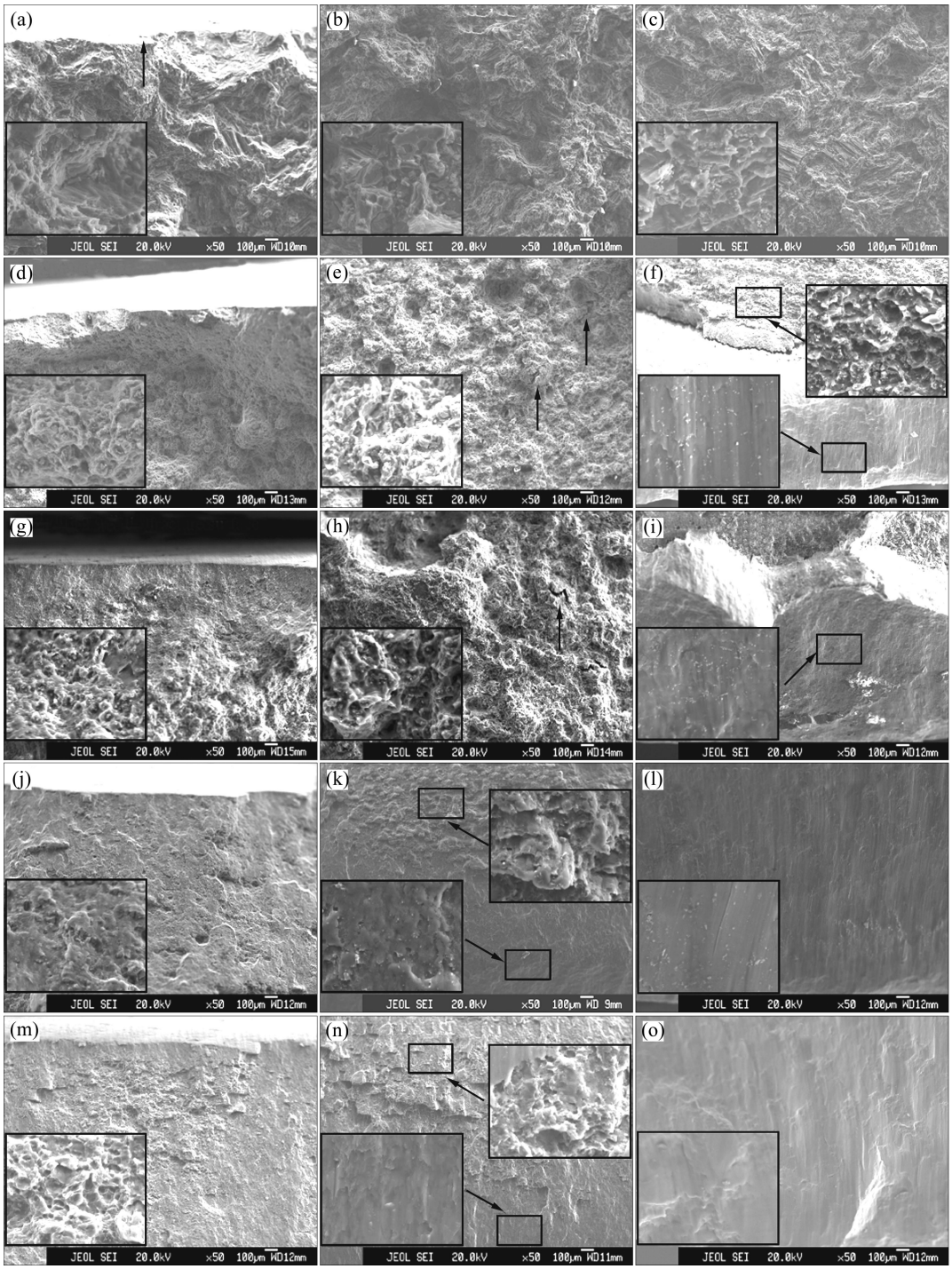

Fig. 7 SEM morphologies for fracture of as-cast (a−c) and extruded (d−o) ZK60−*x*RE alloys (Insets and arrows indicate local magnification and crack, respectively): (a) ZK60−0.30Ho, fracture surface; (b) ZK60−0.30Ho, middle region; (c) ZK60−0.30Ho, impact surface; (d) ZK60−4.77Ho, fracture surface; (e) ZK60−4.77Ho, middle region; (f) ZK60−4.77Ho, impact surface; (g) ZK60−2.98Gd, fracture surface; (h) ZK60−2.98Gd, middle region; (i) ZK60−2.98Gd, impact surface; (j) ZK60−4.32Dy, fracture surface; (k) ZK60−4.32Dy, middle region; (l) ZK60−4.32Dy, impact surface; (m) ZK60, fracture surface; (n) ZK60, middle region; (o) ZK60, impact surface

increases slightly to 15−17 J/cm^2. Although the microstructure is refined significantly after adding high RE content, obviously increased second phase leads to more places for crack initiation. Thus, α_{nK} decreases to 9−10 J/cm^2.

After extrusion, fine grain can consume more energy for crack initiation and propagation. Meanwhile, the broken second phase and many eliminated cast defects can weaken the tendency to intergranular fracture and reduce the place for crack initiation (Figs. 3 and 4).

Therefore, the extruded alloys exhibit the large value of α_{nK}. The extruded alloys with high RE content exhibit smaller grain because more Mg−Zn−RE phase with high thermal stability can inhibit the growth of recrystallization grains effectively compared with those without RE or with low RE content. Thus, the impact toughness should be enhanced significantly in view of grain size. However, more second phase can make crack initiate and propagate along the interface more easily. Taking the two aspects into account, α_{nK} decreases gradually with increasing RE content. The extruded ZK60−4.77Ho alloy exhibits larger second phase in size than the extruded ZK60−4.32Dy alloy, thus the decreasing amplitude in the α_{nK} is more rapid for the former alloy. For the extruded ZK60−2.98Gd alloy, second phase is the most and distributes along the extrusion direction in zonal shape; therefore, its decreasing amplitude in the α_{nK} is the most rapid. It is reflected further that the extruded ZK60 alloy with the largest grain exhibits the largest value of α_{nK} owing to the least second phase. It is proved that the second phase also plays an important role in the impact toughness as well as grain size again. Meanwhile, fine grain and few fine dispersed second phase can enhance other performances such as tensile mechanical property effectively, for example, the tensile strength σ_b and elongation δ can reach 355−395 MPa and 12%−20% at ambient temperature for the extruded ZK60−xRE alloys, respectively.

4 Conclusions

1) With increasing the RE content, the as-cast microstructure is refined gradually. Mg−Zn−RE new phase increases gradually, while $MgZn_2$ phase decreases gradually to disappear. The second phase tends to distribute along grain boundary in continuous network. The extruded microstructure is refined obviously, where the average grain size can reach 1−2 μm for the alloys with high RE content. The broken second phase tends to distribute along the extrusion direction by zonal shape.

2) With increasing the RE content, α_{nK} of as-cast alloys first increases slightly from 13 J/cm^2 to 15−17 J/cm^2 for the alloys with low RE content, and then decreases to 9−10 J/cm^2 for the alloys with high RE content. α_{nK} of the extruded alloys decreases from 54 J/cm^2 to 36, 26 and 28 J/cm^2 for ZK60−4.32Dy, ZK60−4.77Ho and ZK60−2.98Gd alloys, respectively.

3) With increasing the value of α_{nK}, the fracture macro-morphology changes from a rough plane via multi-plane with step to V-type plane; and from single radiation zone to two zones of fiber and shear lip, respectively. The fracture micro-morphology changes from the brittle fracture to the ductile fracture. V-type impact fracture and micro-morphology are formed under the interaction of tensile and tear stresses.

4) To achieve magnesium alloys with high impact toughness and other performances, fine grain and few fine dispersed second phase should be obtained by alloying, amelioration of fabrication condition and so on.

References

[1] POLMEAR I J. Magnesium alloys and applications [J]. Materials Science Technology, 1994, 10(1): 1−14.

[2] PENG B C, ZHANG H X, HONG J, GAO J Q, WANG Q J, ZHANG H Q. Effect of aging on the impact toughness of 25Cr−20Ni−Nb−N steel [J]. Materials Science and Engineering A, 2010, 527: 1957−1961.

[3] MITITITSKY M, MATLOCK D K, REGULLY A, DEWISPELAERE N, PENNING J, HANNINEN H. Impact toughness properties of nickel-free austenitic stainless steels [J]. Materials Science and Engineering A, 2008, 496: 189−199.

[4] MA A B, SUZUKI K, NISHIDA Y, SAITO N, SHIGEMATSU I, TAKAGI M, IWATA H, WATAZU A, IMURA T. Impact toughness of an ultrafine-grained Al-11mass%Si alloy processed by rotary-die equal-channel angular pressing [J]. Acta Materialia, 2005, 53: 211−220.

[5] IBRAHIM M F, SAMUEL E, SAMUEL A M, AL-AHMARI A M A, SAMUEL F H. Impact toughness and fractography of Al−Si−Cu−Mg base alloys [J]. Materials and Design, 2011, 32: 3900−3910.

[6] ELSEBAIE O, SAMUEL A M, SAMUEL F H. Effects of Sr-modification, iron-based intermetallics and aging treatment on the impact toughness of 356 Al−Si−Mg alloy [J]. Journal of Materials Science, 2011, 46: 3027−3045.

[7] ZHANG Xing, ZHANG Zhi-min, LI Bao-cheng. Influence of ageing on impact toughness of AZ80 magnesium alloy [J]. Heat Treatment of Metals, 2007, 32(10): 69−70. (in Chinese)

[8] LI Juan, WANG Wen-xian, ZHANG Lan, SU Juan, ZHANG Hong-xia. Notch impact toughness and fracture mechanism of AZ31 magnesium alloy [J]. Journal of Materials Science & Engineering, 2011, 29(2): 246−251. (in Chinese)

[9] LIAO J S, HOTTA M, KANEKO K, KONDOH K. Enhanced impact toughness of magnesium alloy by grain refinement [J]. Scripta Materialia, 2009, 61: 208−211.

[10] WANG Q D, CHEN W Z, ZENG X Q, LU Y Z, DING W J, ZHU Y P, XU X P, MABUCHI M. Effects of Ca addition on the microstructure and mechanical properties of AZ91magnesium alloy [J]. Journal of Materials Science, 2001, 36: 3035−3040.

[11] SRINIVASAN A, PILLAI U T S, PAI B C. Microstructure and mechanical properties of Si and Sb added AZ91 magnesium alloy [J]. Metallurgical and Materials Transactions A, 2005, 36: 2235−2243.

[12] LIAO J S, HOTTA M, KOSHI A. Effect of oxygen content on impact toughness of a fine-grained magnesium alloy [J]. Materials Letter, 2011, 65: 2995−2999.

[13] VEDANI M. Microstructural and impact toughness properties of a magnesium AM60B die cast alloy [J]. Key Engineering Materials, 2000, 188: 129−138.

[14] SCHMID-FETZER R, KOZLOV A. Thermodynamic aspects of grain growth restriction in multicomponent alloy solidification [J]. Acta Materialia, 2011, 59: 6133−6144.

[15] HUANG Zheng-hua, GUO Xue-feng, ZHANG Zhong-ming, Effects of Ce on damping capacity of AZ91D magnesium alloy [J]. Transactions of Nonferrous Metals Society of China, 2004, 14(2): 311−315.

[16] DEAN J A. Lange's handbook of chemistry [M]. 15th ed. New York: McGraw-Hill Press, 1999.

[17] ZHONG Qun-peng, ZHAO Zi-hua. Fractography [M]. Beijing: Higher Education Press, 2006. (in Chinese)

显微组织对镁合金冲击韧性的影响

黄正华, 戚文军, 徐　静

广州有色金属研究院, 广州 510650

摘　要：分析铸态和挤压态 ZK60−*x*RE(RE=Dy、Ho 和 Gd，*x*=0−5)合金的显微组织，测试其冲击韧性，并讨论两者间的关系。结果表明，随着 RE 含量的增加，铸态组织逐渐细化；Mg−Zn−RE 新相逐渐增多，而 $MgZn_2$ 相逐渐减少直至消失，第二相趋于连续网状分布于晶界处。挤压态组织显著细化至微米级，破碎的第二相沿挤压方向趋于带状分布。冲击韧性值 α_{nK} 由铸态时的 9~17 J/cm^2 提高至挤压态时的 26~54 J/cm^2。随着 α_{nK} 值的增加，断口宏观形貌由一粗糙平面经台阶多面向 V 型面转变，同时由单一放射区向纤维区和剪切唇区组成的两区转变；断口微观形貌由脆性断裂向韧性断裂转变。细小晶粒和细小弥散的第二相将有效提高镁合金的冲击韧性。

关键词：ZK60 镁合金；稀土；合金化；冲击韧性；显微组织；断口形貌

(Edited by YUAN Sai-qian)